Available online at www.sciencedirect.com

ScienceDirect

Procedia Manufacturing 7 (2017) 660 – 667

Procedia MANUFACTURING

International Conference on Sustainable Materials Processing and Manufacturing, SMPM 2017, 23-25 January 2017, Kruger National Park

Surface Texturing of Sialon Ceramic by Femtosecond Pulsed Laser

Lerato Crescelda Tshabalala [a, c], Cebolenkosi Philani Ntuli [a], Jean C. Fwamba[b], Patricia Popoola[a] and Sisa Lesley Pityana [c]

[a]*Tshwane University of Technology, Faculty of Engineering & Built Environment, Department of Chemical, Metallurgical & Materials Engineering, Pretoria, 0001, South Africa*

[b,]*Tshwane University of Technology, Faculty of Engineering & Built Environment, Department of Mechanical Engineering, Pretoria, 0001, South Africa*

[c]*Council for Scientific Industrial Research, National Laser Center, Pretoria, 0001, South Africa*

Abstract

Femtosecond laser surface micromachining is a technique in which an ultrashort pulse laser beam is focused to dimensions of a few microns inside or on the surface of the substrate. In this paper, surface texture transformation behaviour of the SiAlON-Si_3N_4 ceramic using the Ti: Sapphire Femtosecond laser system was investigated. Parametric analysis was conducted using surface drilling, unidirectional and cross-hatching machining procedures performed on the substrate at a varied power and scanning speeds. A linear relation was observed on the microtexturing dimensions and roughness with respect to laser powers and this provided optimum micromachining mechanism at the chosen power of 0.25 W. Two roughness regimes characterised by periodicity and sharp valleys were observed at low pulse overlap and high pulse overlap respectively. Due to the complexity of the surface transformation chemistry, the necessity of a complementary cleaning procedure to remove the silicates retained by the laser treated surface was emphasised.

Peer-review under responsibility of the organizing committee of SMPM 2017

Keywords: Femtosecond laser; SiAlON; Silicon nitride; roughness

1. Introduction

Surface texturing of the cutting tools reduces the contact area between the tool and the chip, ultimately reducing the cutting forces. Surface textures have been produced on the cutting tools by different advanced manufacturing methods like focused ion beam machining and laser technology. The focused ion beam machining has been the most preferred method for accurate positioning and dimensions of the surface textures but it is a time consuming process [1]. The developments in ceramics cutting tool such as silicon nitrides has resulted in considerable increase in productivity and an increased applications in the manufacturing industry.

Peer-review under responsibility of the organizing committee of SMPM 2017

doi:10.1016/j.promfg.2016.12.098

Silicon Nitride (Si_3N_4) based ceramics have undergone numerous advancements in the past four decades, mainly in an attempt to satisfy the industrial needs for superior structural materials. Some recent advances involve the optimisation of critical sintering parameters such as temperature, pressure and the incorporation of various impurity content combinations to re-enforce micro-structural matrices of the components [1-6]. Silicon nitride materials have further developed through the discovery of the alloys that were possible with alumina (Al_2O_3) known as SiAlONs; the name comes from the combination of Si, Al, O and N. The phase that has found the most use in industry is beta sialon, which has the formula Si6-zAlzOzN8-z, where z ranges from 0 (pure beta Si_3N_4) to 4 [2]. The resulting effects have been characterised by other researchers with their findings revealing apparent improvements in mechanical [5-10], chemical [11] and thermal [12] properties. As a consequence, the attractiveness of Si_3N_4 in tribological [10] and most recently, medical [13] applications has significantly improved. Although these attributes make silicon nitrides one of the most promising engineering materials, Si_3N_4 also exhibit low fracture toughness which is attributed to a combination of high hardness and wear resistance alongside their brittle nature. Hence, this makes traditional mechanical machining difficult, uncontrollable, labour intensive and expensive.

A solution to this problem may be the adoption of Femtosecond laser systems since they offer a non-abrasive material removal mechanism at an energy deposition timeframe smaller than the electron-phonon interaction time, leading to a transient, localised energy propagation profile on the irradiated surface. Due to this unique property, ultrashort laser systems have been found to enable melt free material processing, translating to a highest degree of control with minimal damage to the bulk material layers during micromachining of a variety of engineering materials [14-18]. Like in any laser system, the ease of machining is an intrinsic function of the laser parameters and the thermo-physical properties of the material [19].

This paper aims to characterise the surface transformation of the Si_3N_4 ceramic material using the Ti: Sapphire Femtosecond laser system at various parameters of power and scanning speed (pulse overlap) during a large area cross-hatching micromachining procedure. We attempt to achieve this by performing machining threshold estimation trials using the machining dimensions like the ablation diameter and depth. The full surface texturing of the blank cutting tool was used to identify the evolution of various roughness profile to quantify the machining with respect to the chosen parameters. The results and findings highlighted in this paper are important in the fabrication of engineering tools such Si_3N_4 based cutting inserts.

Nomenclature

D_{av}	Average crater diameter
F_0	Gaussian beam maximum fluence
f	Pulse repetition rate
P	Laser beam power
w_0	Laser beam radius at e^{-2} of the maximum intensity
f_{th}	Micromachining threshold fluence
OV	Pulse overlap
V	Scanning speed

2. Experimental Details

2.1. Material

The commercial sintered SiAlON-Si_3N_4 ceramic (Ceramtec International, Germany) was selected as the test material in this study. The properties of the sample are listed in Table 1. The used 4.8x14x14 mm^3 samples had an average as-received surface roughness of $R_a \sim 0.7 \pm 0.05$ µm (measured using a Confocal Laser Scanning Microscope, CLSM).

Table 1. The material properties of the as received Si_3N_4.

Material	α/β SiAlON Wt %	Additives	Density g/cm^3	Conductivity @ 20°C W/m.K	Diffusivity @ 20°C 1/μm
SiAlON-Si_3N_4	19.1	Y_2O_3, MgO, SiC	3.244	23.58	9.69

2.2. Laser system optimisation and Micromachining tests

A regenerative Ti: Sapphire Femtosecond laser system (Spectra Physics, Spitfire) was used to investigate the fundamental conditions for surface roughness modification of the as-received samples. The generated laser pulses (1 kHz) were transported through a series of compensating mirrors. The configured optical system maintained approximately 100 fs as the pulse duration of absorber recovery time in the infrared wavelength of 795 nm with a 16 μm focused beam spot diameter. During the tests, samples were placed on a three-dimensional automated motorized Aerotech stage at a focal length of 45 mm while the beam incident angle was along the normal with respect to the sample. An attenuator was used to obtain proper pulse energy while a power meter was also used to affirm the generated energy. For system optimisation, craters were drilled on the samples at twelve power inputs within the range of 0.2 - 0.75 W using 10 pulses of a fixed laser heat source. These were then used to determine the Micromachining threshold and the machining power range for the experimental design. A Nikon Optical Microscope was used to measure crater diameter, *D* and observe the quality of the drilled craters. Since the craters resembled an elliptical beam distribution in XY domain, the diameter D_x and D_y were measured in the X and Y axis respectively and an average D_{av} was also calculated. Micromachining threshold was calculated using the equations below [20]:

$$F_0 = \frac{2P/f}{\pi w_0^2} \quad (1)$$

$$D^2 = 2w_0^2 ln\frac{F_0}{F_{th}} \quad (2)$$

In equation 1, $F_0\ (J/cm^2)$ is the Gaussian beam maximum fluence, *f (Hz)* represents the pulse repetition rate, *P (W)* is the laser beam power and lastly w_0 is laser beam radius at e^{-2} of the maximum intensity. In equation 2, a relation of the machining crater to $F_{th}(J/cm^2)$, the machining threshold fluence is represented. All the measured machining craters were used to generate a D^2 versus F_o plot to estimate F_{th} at D=0 by the equation 2 for 10 pulses used.

After system optimisation, a large area was ablated at varied power and scanning speed using parameters displayed in Table 2. Different programs were written to enable the patterning strategies using cross-hatching at a two dimensional scan spacing of 0.0128 mm. The samples were created using two scan speeds, 8 and 4 mm/s, by a unidirectional scanning strategy to achieve 50% overlap (2 successive pulses per spot) and 75% overlap (8 pulses per spot) respectively. In equation 3, the overlap, (OV) between pulses is defined from laser operated at 1 kHz with a fixed focused laser spot diameter ($2w_0$) of 16 um as in equation.

$$OV = (1 - \frac{v}{2fw_0}) \quad (3)$$

Where *v (mm/s)* and *f (Hz)* are scanning speed and laser pulse repetition rate respectively. For all tests, only the scanning speed was altered to change the pulse overlap.

In order to optimise machining threshold for removing a 5 – 10 μm layer on the material on full machining of the surface. The interactions between processes variables were analysed using the response surface method in a factorial

design on numeric factors (see Table 2). The numeric factors were laser power and scanning speed. Process characterisation was performed using roughness parameters Ra, Rsk, Rz for overall surface profiling measured by the Confocal laser Scanning Microscope (CLSM).

Table 2. The machining design summary extracted from Design Expert 8.

Factor	Name	Units	Type	Minimum	Maximum	Mean	Std. Dev
A	Power	W	Discrete	0.1	0.5	0.28	0.18
B	Speed	mm/s	Discrete	4	16	10	3.34

Response	Name	Units	Analysis	Minimum	Mean	Maximum
Y1	Ra	µm	Polynomial	0.40	0.65	0.90
Y2	Rz	µm	Polynomial	1.50	3.25	5.00
Y3	Rsk	µm	Polynomial	-0.74	-0.22	0.30

3. Results and Discussions

3.1. Laser system optimisation

The ablated craters at 10Hz frequency, (10 pulses) at power range between 0.2 W and 0.75 W providing linearity in crater diameter, D with an increase in fluence calculated form the various laser power inputs as displayed on the plot on fig 1. An extrapolations was conducted in fig 1 at D_2=0 indicated that the machining threshold for the SiAlON- Si_3N_4 was about 26 J/cm2 (0.05 W) for the utilized femtosecond laser system. The machining was due to a single mechanism which is characterized by gentle material removal rates due to particle vaporization i.e Coulomb explosion phase was exhibited [21-22]. The combination of high peak intensity and ultrashort energy dissipation time frame induced sufficient energy distribution in the form of heat during absorption on the irradiated zone causing localized direction phase transition from solid to vapor at energies around the machining threshold [23].

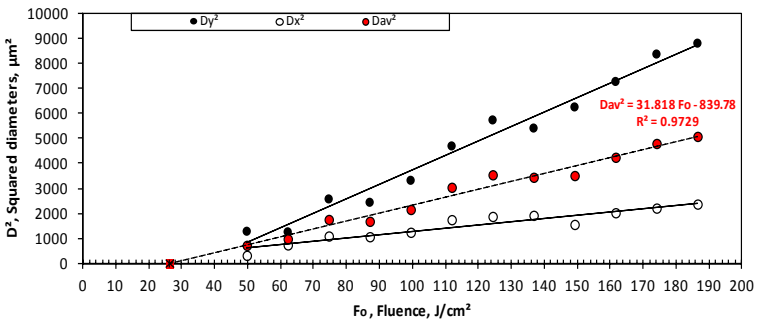

Fig. 1. Squared crater diameter of SiAlON-Si_3N_4 sample.

Fig 2 a-c represents the machining depth (Hz) from the results obtained for the 3x3mm^2 regions using the unidirectional scanning strategy. This was a moving laser heat source instead of the stationery heat source used during machining crater creation. When a moving heat source is used, the material is subjected to a transient thermo-physical phenomena which result in a physical texture determined by laser parameter induced for material removal (power, pulse repetition, scanning speed and the pulse over overlap) [24] . Due to a higher pulse overlap of 88% obtained at 2 mm/s scanning speed, a steeper machining depth creation slope of 69.89µm/W was obtained while a 32.88 µm/W was estimated when a 50% overlap at 8 mm/s. This relation demonstrated that longer laser-material interaction time results to high material removal profiles while at the lowest pulse overlap the opposite was

observed. Thus, this concluded that there was a high dependency of the material removal rate on both power and pulse overlap machining factors [24-26].

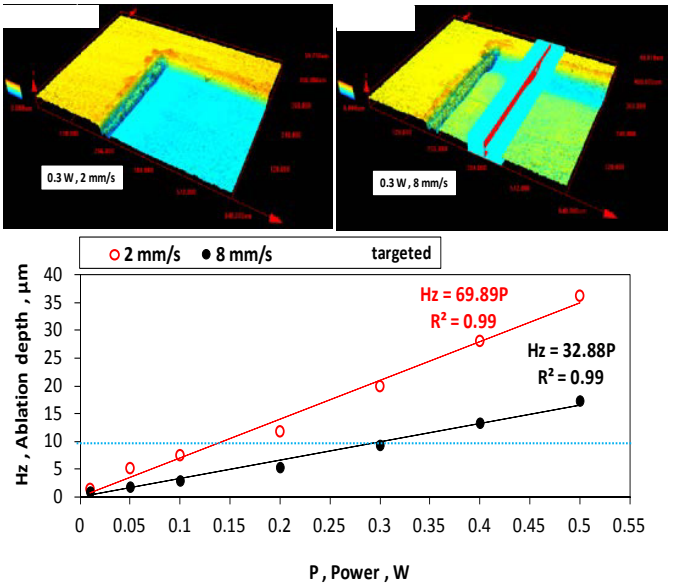

Fig. 2. Machining depth results obtained from the 3x3 mm^2 ablated regions with a unidirectional scanning strategy at 0.3 W and a scanning speed of (a) 8 mm/s, (b) 2 mm/s and (c) the plots of all the measured machined depths.

Fig 3 represents the overall surface topography with respect to Ra (3D arithmetic mean roughness), Rz (mean depth of the valleys) and Rsk (skewness of the peaks for the formed profile) at different combinations of laser power and scanning speed. Surface transformation by a laser power of 0.25 W at a scanning speed of 4 to 16 mm/s was also observed. The rougher surface evolution was obtained when scanning speeds of 4 – 8 mm/s were used. There was an increase in the periodicity of the profile at a scanning speed of 8 mm/s characterised by sharper peaks and lower valleys. This regime can be attributed to the high laser-surface interaction time accompanied by high material removal.

An increase in the Rz values from 4.668µm to 5.391µm (see fig 4b) is indicative of the surface transformation that leans towards an increase in the sharpness of the valleys observable from a 12-16mm/s regime. At high scanning speeds, there was a reduction in the wavy character of the surface while the Rsk values (fig 4c) increment was indicative of the sharpness of the valleys. The observed surface profiles show the evidence of the two machining regimes induced by the laser system which have high sensitivity to the chosen scanning speed and laser power.

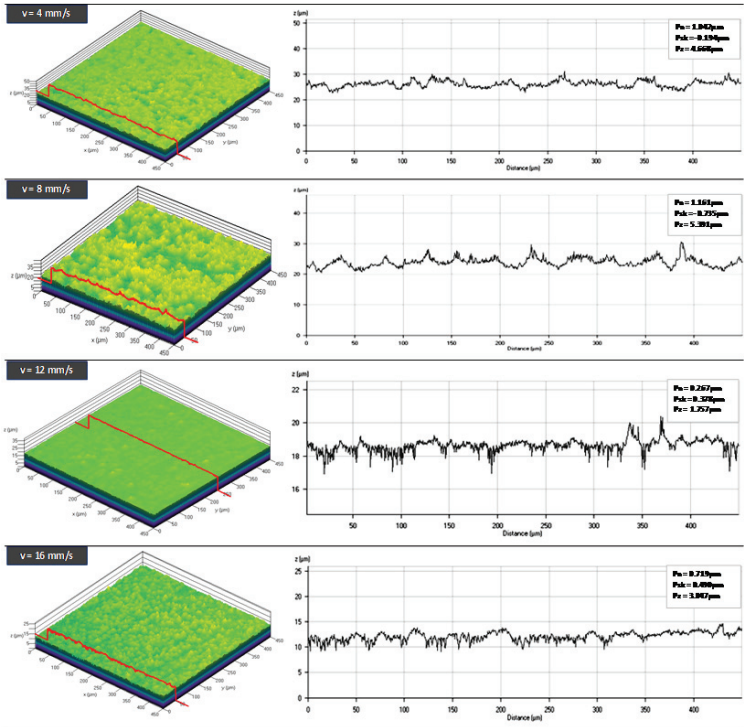

Fig. 3. The Confocal Laser Scanning Microscope images of the fully ablated surfaces by cross hatching at 0.25 W using speeds of 4 - 16 mm/s (0.88 down to 0 pulse overlap).

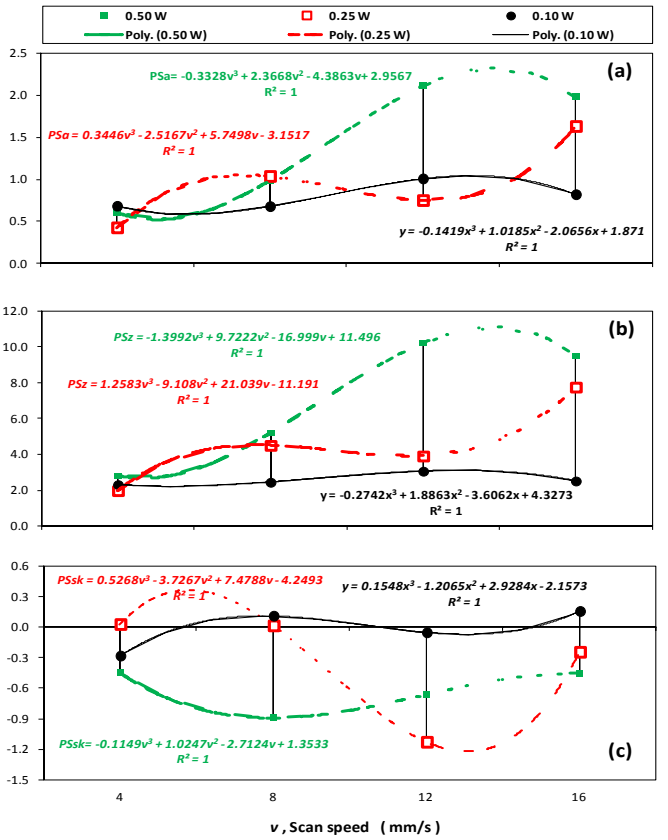

Fig. 4: Mean surface roughness profiles [a) Ra, b) Rz, c) Rsk] created using a Ti:Sapphire femtosecond laser at different power (0.1 - 0.5 W) and scanning speed (4 - 16 mm/s) on a SiAlON-Si_3N_4 sample by cross-hatching scanning strategy.

4. Conclusion

Surface transformation of SiAlON-Si_3N_4 sample using a femtosecond Ti: Sapphire in air was successful. After machining the following conclusions were drawn:

- The craters drilled using 10 pulses at a power range of 0.1 - 0.75 W showed linearity to an increase in laser power.
- A single machining regime attributed to coulomb explosion was exhibited at the chosen machining laser power range with the machining threshold was estimated to be 26 J/cm^2 (0.05 W).
- At low scan speeds (high pulse overlap), high material removal slopes could be obtained while the opposite was true for high speeds (low pulse overlap). Although high powers induced high material removal, in large area micromachining by cross-hatching, two roughness regimes were observed: at low scan speeds (2 -8 mm/s), the transformed surface had high periodicity while of the sharp valleys were observed at high scan speeds (12-16 mm/s). Thus the resulting topography showed high dependence to pulse overlap.

Acknowledgements

The authors would like to acknowledge the contributions from the Fraunhofer Institute for Surface Engineering and Thin Films, CSIR Rental Pool Program and the Faculty of Engineering and Built Environment at Tshwane University of Technology for the facilities and financial support towards this project.

References

[1] I. Upadhyay and P. Rathod, Performance evaluation of textured cutting tools – a review, International journal of engineering development and research 4[1] (2016): 231 – 241.

[2] S. Hampshire, Silicon nitride ceramics – review of structure, processing and properties, Journal of achievements in materials and manufacturing engineering 24[1] (2007): 43-50.

[3] A.H. Jones, and K. Hudson, Enhanced Sialon-Bonded Silicon Carbide, http://www.ceramicindustry.com/articles/93850-enhanced-sialon-bonded-silicon-carbide (2014)

[4] Z-H. Xie, R. J. Moon, M. Hoffman, P. Munroe, Y-B. Cheng, Role of microstructure in the grinding and polishing of α-sialon ceramics, Journal of the European Ceramic Society 23 (2003): 2351-2360.

[5] K.P. Pluckenett, M. Quinlan, L. Garrido, L. Genova, Microstructural development in porous B-Si_3N4 ceramics prepared with low volume RE_2O_3-MgO-CaO additions (RE=La, Nd, Y, Yb), Materials science and engineering A 489 (2008): 337-350

[6] C.C. Guedes-Silva, F.M. de Souza Carvalho, J.C. Bressiani, Effect of rare-earh oxides on properties of silicon nitride obtained by normal sintering and sinter-HIP, Journal of rare earhs 30 [11] (2012): 1177.

[7] H-H. Lu, J-L. Huang, Effect of Y_2O_3 on the microstructure and mechanical properties of silicon nitride, Ceramics international 27 (2001): 621-628.

[8] I. Ganesh, Development of β-SiAlON based ceramics for radome applications – Review paper, Processing and application of ceramics 5 [3] (2011): 113-138.

[9] C.P. Dogan, J.A. Hawk, Microstructure and abrasive wear in silicon nitride ceramics, Wear 250 (2001): 256-263.

[10] M.H. Bocanegra-Bernal, B. Matovic, Mechanical properties of silicon nitride-based ceramics and its use in structural application at high temperatures, Materials science and engineering A 527 (2010): 1314-1338.

[11] T. Rouxel, J-C. Sangleboeuf, M. Huger, C. Gault, J-L. Besson, S. Testu, Temperature dependence of Young's modulus in Si_3N_4-based ceramics: roles of sintering additives and of SiC-particle content, Act Materialia 50 (2002): 1669-1682.

[12] K. Thoma, L. Rohr, H. Rehmann, S. Roosm J. Michler, Materials failure mechanisms of hybrid ball bearings with silicon nitride balls, Tribology 37 (2004): 463-471.

[13] H. Park, H-W. Kim, H-E. Kim, Oxidation and strength retention of monolithic Si3N4 and nanocomposite Si_3N_4 with Yb_2O_3 as a sintering aid, J. Am. Ceram. Soc. 81 [8] (1998): 2130-2134.

[14] I. Khader, A.Renz, A. Kailer, D. Haas, Thermal and corrosion properties of silicon nitride for copper die casting components, Journal of the European Ceramic Society 33 (2013): 593-602.

[15] R. Le Harzic, R. Buckle, C. Wullner, C. Donitzky, K. Kong, Laser safety aspects for refractive eyes surgery with femtosecond laser pulses, Medical laser application 20 (2005): 233-238.

[16] B.S. Bal, M.N. Rahaman, Orthopedic applications of silicon nitride ceramics, Acta Biomaterialia 8 (2012): 2889-2898.

[17] P.J. Ding, Q.C. Lui, X. Lu, X.L. Liu, S.H. Sun, Z.Y. Liu, B.T. Hu, Y.H. Li, Hydrodynamic simulation of silicon ablation by ultrashort laser irradiation, Nuclear instruments and methods in physics research B 286 (2012): 40-44.

[18] Y. Xing, J. Deng, Y. Lian, K. Zhang, G. Zhang, G. Zhang, J. Zhao, Multiple nanoscale parallel grooves formed on Si_3N_4/TiC ceramic by femtosecond pulsed laser, Applied surface science 289 (2014): 62-71.

[19] S.Y. Wang, Y.Ren, C.W. Cheng, J.K. Chen, D.Y. Tzou, Micromachining of copper by femtosecond laser pulses, Applied surface science 265 (2013): 302-308.

[20] C. Momma, S. Nolte, B.N. Chichkov, F.V. Alvensleben, A. Tunnermann, Precise laser ablation with ultrashort pulses, Applied surface science 109/110 (1997): 15-19.

[21] A.N. Samant, N.B. Dahotre, Laser machining of structural ceramics- a review, Journal of the European ceramic society 29 (2009): 969-993.

[22] L. Qi, K. Nishii, M, Yasui, H. Aoki, Y. Namba, Femtosecond laser ablation of sapphire on different crystallographic facet planes by single and multiple laser pulses irradiation, Optics and lasers in engineering 48 (2010): 1000-1007

[23] R. Stoian, A. Rosenfeld, D. Ashkenasi, I. Hertel, N. Bulgakova, E.E.B. Campbell, Surface charging and impulsive ion ejection during ultrashort pulsed laser ablation, Phys. Rev. Lett 2002: 88: 097603.

[24] Y. Ren, J.K. Chen, Y. Zhang, Modelling of ultrafast phase changes in metal films induced by an ultrashort laser pulse using a semi-classical two-temperature model, International journal of heat and mass transfer 55 (2012): 1620-1627.

[25] P.T. Mannion, J. Magee, E. Coyne, G.M. O'connor, T.J. Glynn, The effects of damage accumulation behaviour on ablation thresholds and damage morphology in ultrafast laser micro-machining of common metals in air, Appl. Surf. Sci. 233 (2004): 275-287.

[26] N.M. Bulgakova, I.M. Bourakov, Phase explosion under ultrashort pulsed laser ablation: modelling with analysis of metastable state of melt, Applied surface science 197-198 (2002): 41-44.

[27] P. Parandoush, A. Hossain, A review and simulation of laser beam machining, International journal of machine tools and manufacture 85 (2014): 135-145.